CHAPTER EIGHT

Fermi Surface Calculations and Analysis

8.1 Introduction

When a solid possessing a partially filled band is a normal metal (i.e., when the electrons of the partially filled band are not localized), the wave vectors of its FPZ are divided into occupied and unoccupied wave vectors (see Chapter 4). The Fermi wave vectors $\mathbf{k}_F$ form the boundary between the occupied and unoccupied wave vector regions, and such boundary surfaces are known as Fermi surfaces. All crystal orbital energies calculated for a set of k-points sampling the FPZ are stored in a *filename.BE* file, which is used to construct the Fermi surfaces of partially filled bands.

For 1D chain calculations carried out with a set of k-points in 1D FPZ, the Fermi surface is given by two points $\mathbf{k}_F$ and $-\mathbf{k}_F$. This information is readily obtained when the band dispersion relations are plotted in the vicinity of the Fermi level by running the *PP* program. The Fermi surface calculation program *FC* is used only when electronic band structure calculations are carried out for a 2D layer or a 3D solid.

The *FC* program generates Fermi surface contours for every partially filled band on certain cross-section planes of the FPZ specified by the user. It requires an input file *filename.FI* and the *filename.BE* file produced by the *BC* program. A Fermi surface of a 3D solid is constructed by combining the Fermi surface contours obtained for a number of cross-section planes slicing the 3D FPZ. These planes are chosen to be parallel to a plane defined by two of the three reciprocal vectors (e.g., a^*b^*-plane), and their heights along the remaining vector (e.g., c*) are chosen at certain regular intervals (e.g., 0.0, 0.1, 0.2, 0.3, 0.4, 0.5 in units of c*). Note the convention that the a^*b^*-, b^*c^*- and a^*c^*-planes are termed the XY-, YZ- and XZ-planes, respectively.

The *FC* program generates two output files, *filename.FO* and *filename.FG*. The latter is used by the *FP* program to display the calculated Fermi surfaces.

8.2 Fermi surface calculation program *FC*

The parameters necessary for Fermi surface calculations are stored in an input file, *filename.FI*. The *FC* program reads in the energy levels $e_i(\mathbf{k})$ of partially filled bands from the *filename.BE* file, generates analytical expressions for the $e_i(\mathbf{k})$-vs.-$\mathbf{k}$ relationships using the cubic spline fitting method, and then determines Fermi surface contours lying on the cross-section planes of the FPZ specified by the user.

8.2.1 Input file *filename.FI*

When the *NEWFI* program is launched, it opens the *New. FI File* dialog box (*Figure 8.1*). The items of this dialog box are described below.

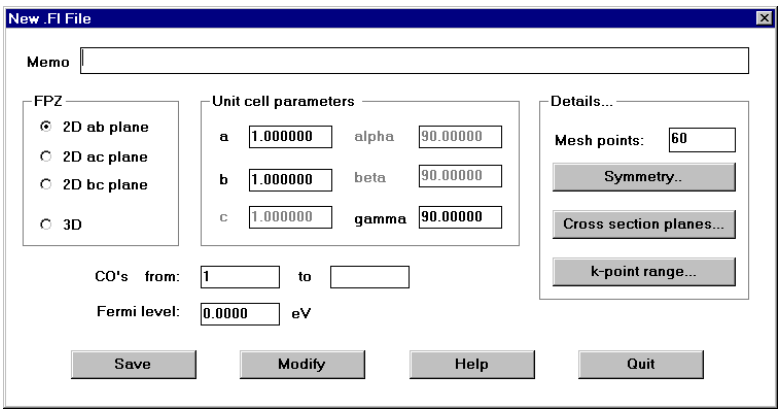

Figure 8.1. New .FI File dialog box.

•*Memo*

This is used to briefly describe a computational task.

•*FPZ*

This field is used to specify whether the *BC* program was run for a 3D lattice or an isolated 2D layer. For the case of a 2D layer, it is necessary to indicate whether the layer is parallel to the *ab*-, *ac*- or *bc*-plane of the 3D solid from which it is taken.

•*Unit cell parameters*

The vectors **a***, **b*** and **c*** of the reciprocal space are defined by the vectors **a**, **b** and **c** of the real space. Thus the parameters of the real-space unit cell should be provided in the *Unit cell parameters* field. If the *BC* program was run for a 2D layer, the user should specify only the two vectors and the angle between them defining the layer. For example, for a layer parallel to the *ab*-plane, the required parameters are ***a***, ***b*** and *g*.

•*Fermi level*

The Fermi level e_f corresponding to the total number of valence electrons per unit cell. The user can find this value at the end of a *filename.BO* file or near the beginning of a *filename.PO* file.

•*CO's*

The sequence numbers of the partially filled bands. They are found by plotting band dispersion relations around the Fermi level using the *PP* program. (Note that each completely filled band contains two electrons per unit cell for a normal metallic solid.) For a system with several partially filled bands, it may be necessary to know the Fermi surface for each partially band. In this case, the user should run the *FC* program several times by specifying one band in the *CO's* field.

•*Details...*

This field is used to define the number of mesh points, the symmetry operations for generating the k-points covering the whole FPZ, the cross-section planes for Fermi surface contour calculations, and the range of k-points needed for plotting the Fermi surface contours.

Mesh points:

To calculate the Fermi surface of a partially filled band, it is necessary to know its orbital energies at a large number of mesh points of the FPZ, much larger than the set of k-points actually used in running the *BC* program. This requires a cubic spline fitting of the calculated band energies as a function of k-points. Based on the resulting analytical expressions of the $e_i(\mathbf{k})$-vs.-$\mathbf{k}$ relationships, the values of band energies are calculated at a large number of mesh points covering the FPZ. The default value of the mesh points is 60, namely, half the length of each reciprocal vector of the FPZ (e.g., $0.0 \le k_a \le 0.5$) is divided into 60 equidistant k-points.

Symmetry...:

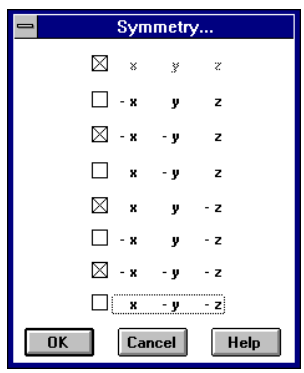

Figure 8.2. Symmetry operations for an orthorhombic system.

The symmetry operations for k-points are needed to generate the k-points covering the whole FPZ from a set of k-points defined for part of the FPZ. This button opens the *Symmetry...* dialog box (*Figure 8.2*), where (x y z) refers to the identity operation. The *FC* program provides 2 or 4 symmetry operations for a 2D layer, and 4 or 8 symmetry operations for a 3D lattice. Based on these symmetry operations and the energy levels stored in the *filename.BE* file, the energies of partially filled bands are made available for k-points throughout the whole FPZ. For example, suppose that *BC* was run for the k points sampling the first quadrant of a 2D FPZ. Then four operations, (x, y, z), (x, -y, z), (-x, y, z), and (-x, -y z), should be chosen from the symmetry table.

Cross-section planes:

This button opens the *Cross-section planes...* box, which is used to specify the cross-section planes for Fermi surface calculations (*Figure 8.3*). For example, in *Figure 8.3*, only the a*b*-plane (i.e., XY-plane) is highlighted because the *New .FI File* dialog box (*Figure 8.1*) defines Fermi surface calculations for a 2D layer parallel to the *ab*-plane.

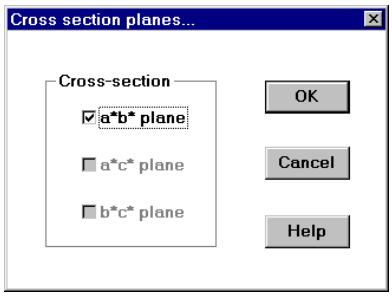

Figure 8.3. Cross section planes... dialog box.

k-point range...:

This button opens the *k-point range* dialog box (*Figure 8.4*), which is used to define the area or the volume of the reciprocal space in which to draw the Fermi surface. For example, consider Fermi surface calculations for a 3D solid on the cross-section plane parallel to the a*b*-plane that intersects the c*-axis at 0.1c*. Then the dialog box should be specified as shown in *Figure 8.4*. This option is useful when it is desired to obtain a Fermi surface in a reduced part of the FPZ.

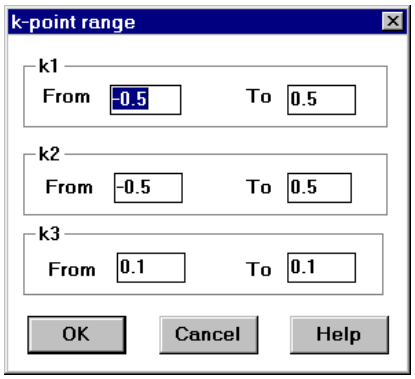

Figure 8.4. Specification of the cross-section plane parallel to the a*b*-plane and intersecting the c*-axis at 0.1c*.

According to the k-space convention for a 2D layer discussed in Chapter 5, the k-point range for a 2D layer is specified using the fields reserved for the a*b*-plane, even when the layer is parallel to the *ac*- or *bc*-plane of the solid.

Since the *FP* program can repeat a Fermi surface calculated for the FPZ along the **a***-, **b***- or **c***-directions, it is unnecessary to calculate Fermi surfaces beyond the FPZ. With the default setting, *FC* performs Fermi surface calculations only within the FPZ.

8.2.2 Editing an input file

An experienced user may create a new input file, *filename.FI*, by `modifying an` existing one. This can be achieved by using any text editor or by using the *Modify* command of the *New .FI* dialog box. When clicked, it opens the *Open* dialog box to allow the user to locate the existing file and copy its contents into the parameter fields of *New .FI File* dialog box. Then the user can edit the file by going through the appropriate fields of the *New .FI File* dialog box where changes have to be made.

8.2.3 Output files of *FC*

The *FC* program generates two output files, *filename.FO* and *filename.FG*. The *filename.FO* file summarizes all information concerning the input data file and all k-points used for Fermi surface calculations. The *filename.FG* file includes all data needed for plotting the calculated Fermi surfaces on screen by the *FP* program.

8.2.4 Limitations of *FC*

Although dynamic memory management is employed in *FC*, there are still a few limitations to note. For a Fermi surface of a 3D solid, the maximum number of cross-section planes along each direction of the three reciprocal vectors is limited to 50. In most cases, 6 planes in each direction generates a clear picture of any Fermi surface in 3D FPZ. Use of too many planes may reduce the clarity of a 3D perspective, since the picture is made up of the contours on the cross-section planes.

8.3 Fermi surface display program *FP*

8.3.1 Display and analysis options of *FP*

When the *FP* program is loaded with a proper *filename.FG* file, the *FP* window appears (*Figure 8.5*). The menus of this window include *View*, *Stereo*, *Extend*, *Zoom*, *Preference*, *Rotation*, *Save* and *Help*. The functions of these menus are described below.

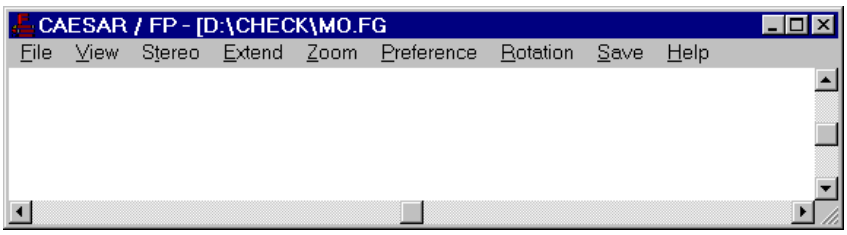

Figure 8.5. Window of *FP*.

• ***View***

When this menu is clicked, the calculated Fermi surface is displayed on the screen under the default setting. It has two commands, i.e., *Within unit cell* and *Shift* (*Figure 8.6*).

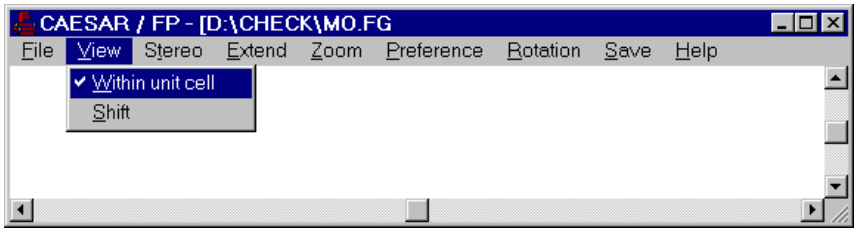

Figure 8.6. Items of the *View* menu.

Within unit cell:

This command shows the Fermi surface such that the Γ point is used as the center of the picture representing the Fermi surface.

Shift:

This command shifts the center of the picture representing the Fermi surface can be shifted to another k-point. It opens the *Surface center shift* dialog box (*Figure 8.7*), which is used to define a new center around which to display the Fermi surface. For example, the example of *Figure 8.7* shifts the center to the R = (0.5, 0.5, 0.5) point.

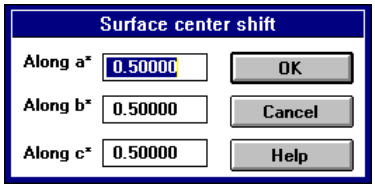

Figure 8.7. Surface center shift dialog box.

The *Shift* option is useful for cases when a Fermi surface is centered around corners and edges of the FPZ, because it enables one to see the overall shape of a Fermi surface more clearly. To find to where the center should be shifted, it is necessary to examine each cross-section view of the Fermi surface separately.

•*Stereo*

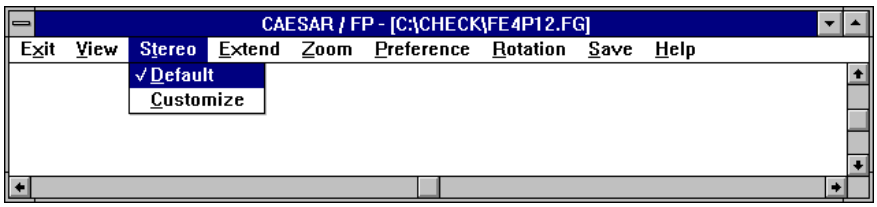

Figure 8.8. Items of the *Stereo* menu.

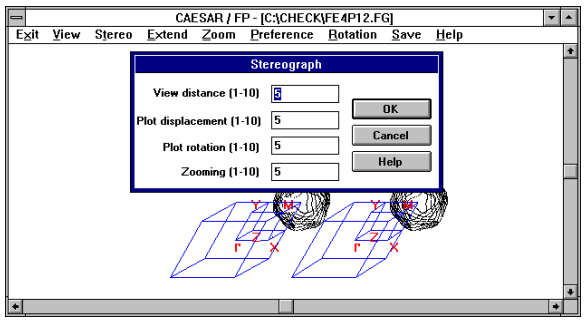

Figure 8.9. Stereograph dialog box.

This menu allows the user to obtain a stereoview of the calculated Fermi surface (*Figure 8.8*). It has two commands, *Default* and *Customize*. The parameters for producing stereographic effect can be taken from the default values using the *Default* command or can be specified by using the *Customize* command. The latter opens the *Stereograph* dialog box (*Figure 8.9*), which has four parameters to specify. These parameters can take values from 1 to 10. When the *Stereo* menu is in use, the *Zoom* menu of the *FP* window is disabled. Therefore, for large and improperly oriented Fermi surfaces, the

left and right diagrams of a streoview pair can overlap thereby resulting in a unclear stereoview. In such cases, one should redefine the values of *Plot displacement* and the *Zooming factor* in the dialog box to make the diagrams farther apart and smaller.

•*Extend*

To examine the topological features of a Fermi surface such as connections, channels and nesting, it is convenient to repeat its satisfactory view that is obtained after zooming or rotating. Fermi surfaces in 2D FPZ can be repeated only along the a*-and b*-directions, and those in 3D FPZ can be extended in any direction. During the extending operation, the rotation function is suppressed and the vector logo disappears. If it is needed to extend a Fermi surface with a specifically orientated view, the Fermi surface should be rotated beforehand. This menu has three groups of commands, as shown in *Figure 8.10*. The items in the second group define the plane(s) where the extension operation will take place.

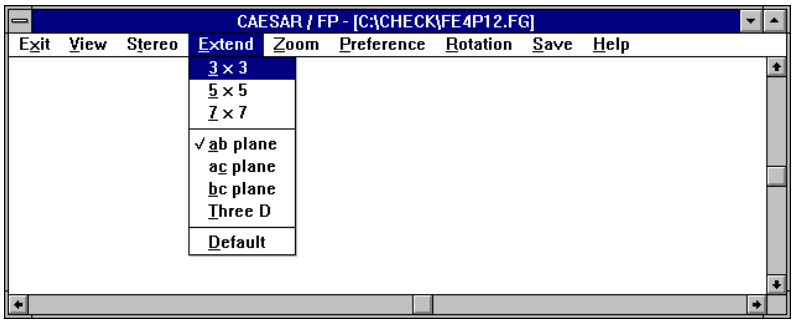

Figure 8.10. Items of the *Extend* menu.

•*Zoom*

This menu provides three commands, *Zoom Out*, *Zoom In* and *Default* (*Figure 8.11*), which can be used to reduce or enlarge the size of the Fermi surface display on the screen.

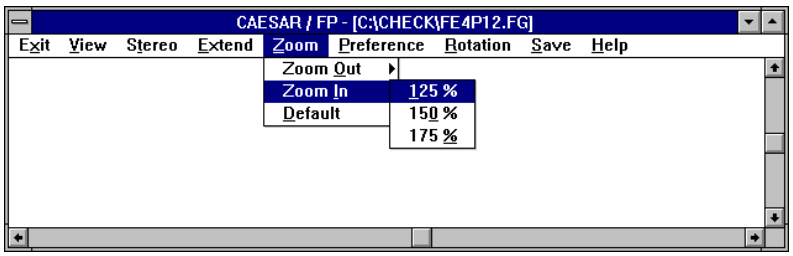

Figure 8.11. Items of the *Zoom* menu.

•*Preference*

The features of graphics can be reset by selecting appropriate commands of the *Preference* menu (*Figure 8.12*).

Line style:

This command is used to select styles of curves (i.e., *dotted*, *circled* or *solid*) for plotting Fermi

surface contours. There are three different radii for circles. The *Solid* option provides three choices to ensure the continuity of solid lines for Fermi surface contours. In most cases, the *Default gap* gives satisfactory, continuous solid curves. If there are still gaps left along a contour line, one might try the option *2 x gap* or *3 x gap*.

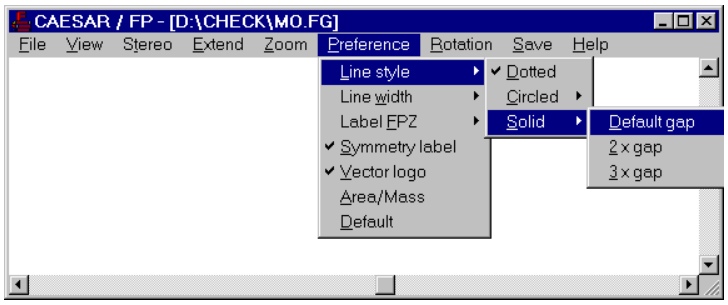

Figure 8.12. Items of the *Preference* menu.

Line width:

This provides three choices of line widths, with which to draw both curves and the unit cell box.

Label FPZ:

This option enables the user to display the FPZ in different ways (*Figure 8.13*). The option *3D* draws the 3D FPZ. Sometimes it is necessary to see a projection view of Fermi surfaces on a specific plane. The options *xy(3D)*, *yz(3D)* and *zx(3D)* displays a 3D FPZ as its projection view on the a*b*-, b*c*- and a*c*-planes, respectively.

For Fermi surfaces of an isolated 2D layer, the *FC* program always assigns the first and second directions of the 2D FPZ to **a*** and **b***, respectively. With respect to the repeat vectors of a 3D solid from which a single layer is isolated, the Fermi surface of this layer may lie on a plane other than the *a*b**-plane. For example, the layer is parallel to the *bc*-plane, so that its Fermi surface should be in the *b*c**-plane. For such a case, it is necessary to modify the symmetry labels of the FPZ for presentation purposes. The six options from *xy(2D)* to *zy(2D)* provide different ways of labeling the 2D FPZ.

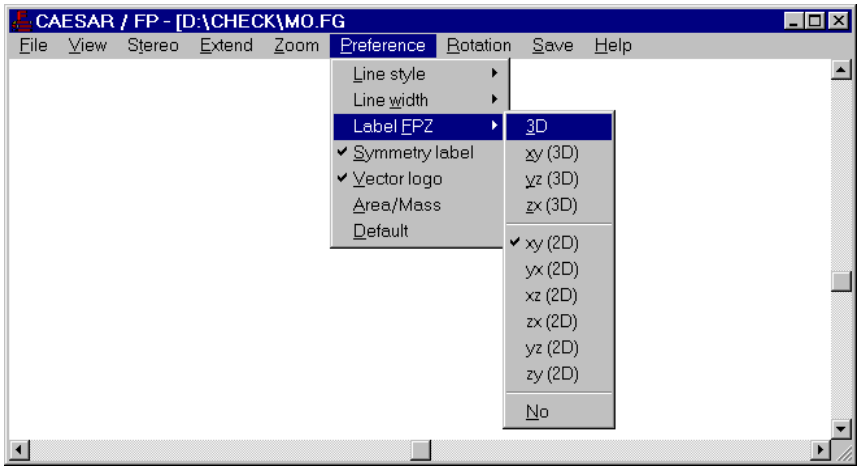

Figure 8.13. Options of the *Preference: Label FPZ* command.

Area/Mass:

For a Fermi surface in 2D FPZ possessing electron and hole pockets, the percentages of their areas with respect to the whole FPZ area as well as their effective masses are useful quantities in analyzing magnetoresistance properties. When the *Area/Mass* command allows the user to calculate these quantities.

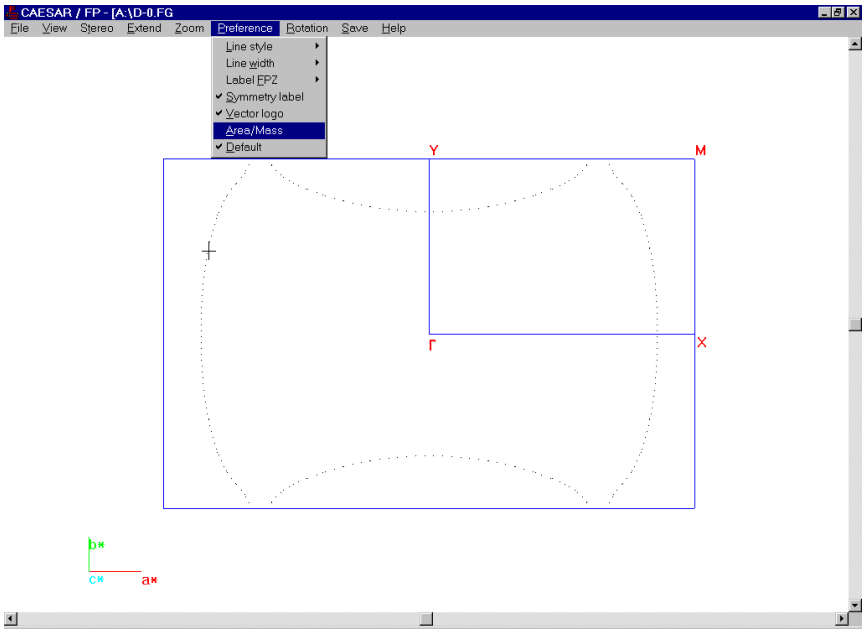

Figure 8.14. Area/Mass command of the *Preference* menu.

When this command is selected, the cursor's shape changes to a cross mark (*Figure 8.14*) to enable the user to select a Fermi surface contour by positioning the cursor center on any part of the contour and then clicking it. This opens the *Area/Mass Information* dialog box (*Figure 8.15*), which provides information about the sequential number of the associated band level, the Fermi level, the orientation of the cross-section plane, the height of this plane along the third reciprocal vector, and the sizes of the occupied and unoccupied wave vector regions in percentiles of the FPZ.

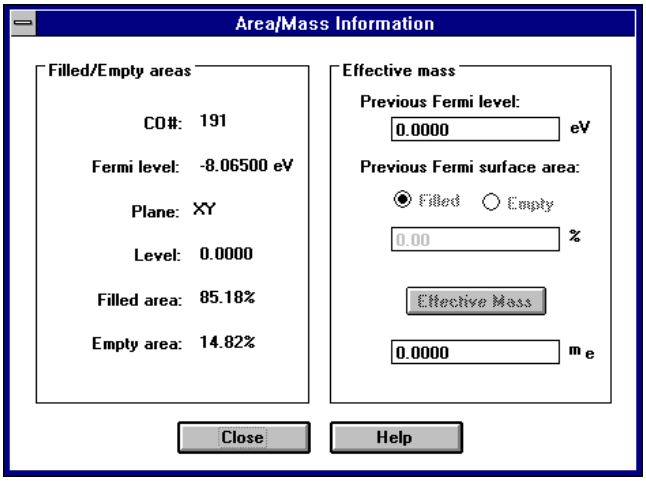

Figure 8.15. Area/Mass information dialog box of the *Preference: Area/Mass* command.

Given a Fermi surface contour on a cross-section plane, the average effective mass m^* associated with the contour at the Fermi level e_f can be calculated according to Eq. 4.74. The term d*A*/de can be evaluated by calculating the Fermi surface area *A* of the filled (or empty) wave vector region (in % of the cross-section area of the FPZ) at e_f and $e_f - \delta\varepsilon$ or at e_f and $e_f + \delta\varepsilon$, where $\delta\varepsilon$ is a small number (e.g., 0.01 eV). Therefore, Fermi surface calculations should be performed by running the *FC* program once with e_f as the Fermi level and immediately afterward with $e_f - \delta\varepsilon$ (or $e_f + \delta\varepsilon$) as the Fermi level. The *Effective Mass* button is activated in the second (i.e., current) calculation by entering the Fermi level and the Fermi surface area calculated in the first (i.e., previous) calculation. Click the *Effective Mass* button to display the effective mass. By repeating the above procedure, one can obtain the information about any Fermi surface contours on a cross-section plane.

It is also possible to calculate the areas and effective masses associated with any cross-section view of a Fermi surface in 3D FPZ.

•*Rotation*

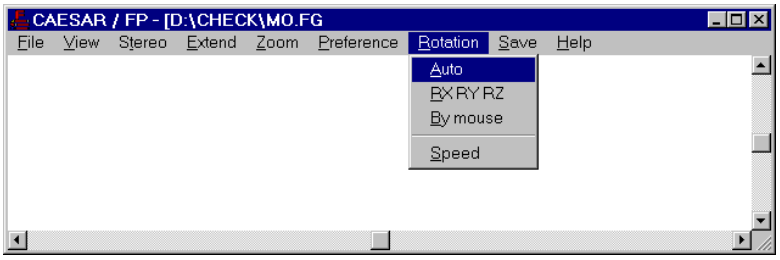

Figure 8.16. Items of the *Rotation* menu.

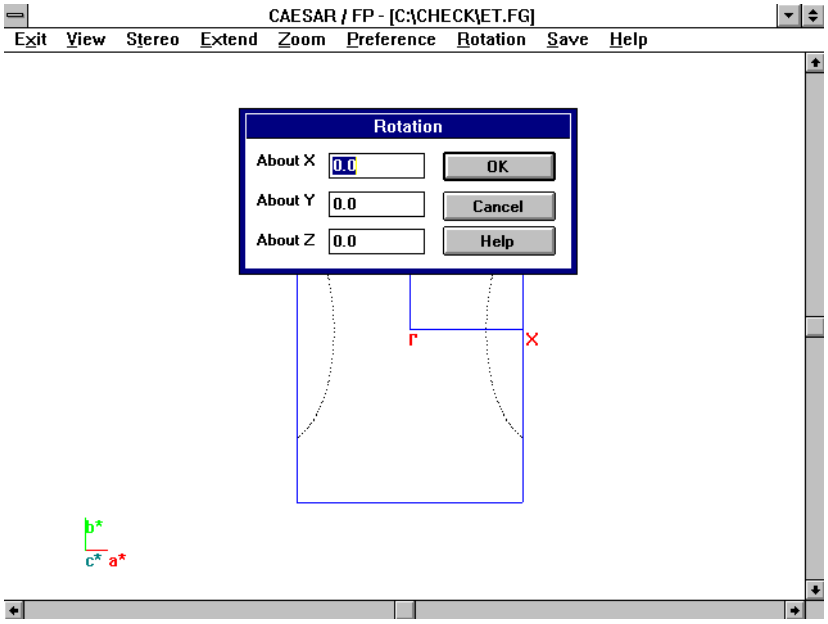

Figure 8.17. Rotation dialog box of the *Rotation: RX RY RZ* command.

This command allows the user to rotate a displayed Fermi surface. It provides four other

commands, i.e., *Auto*, *Rx Ry Rz*, *By mouse* and *Speed* (*Figure 8.16*). The *Auto* command initiates a series of continuous rotations in the 3D space. The rotation stops immediately once a mouse button or any key is pressed. The *Rx Ry Rz* command opens the *Rotation* dialog box (*Figure 8.17*). A desired rotation is defined by specifying the rotational angles around the three coordination axes. The *By mouse* command allows the user to rotate a displayed Fermi surface interactively by the mouse drag method. When clicked, the *Speed* command opens the *Rotation speed* dialog box (*Figure 8.18*). The user can enter a proper value in the *Speed* field to get a smooth movement. The user can also click the horizontal and vertical scroll bars of the *FP* window to rotate a displayed Fermi surface interactively.

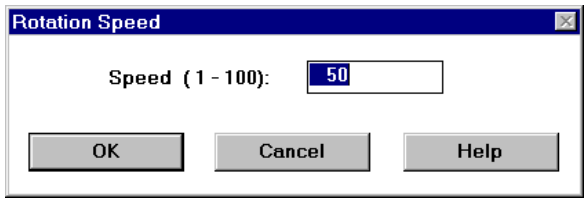

Figure 8.18. Rotation Speed dialog box.

•*Save*

This command is used to capture the content in the current window and save it in a PostScript file *filename.FP* by opening the *Save As* dialog box (*Figure 8.19*). Several different pictures can be saved in one *filename.FP* file. Each picture is saved as one full page. Once a *filename.FP* file is created, many pages can be appended to it.

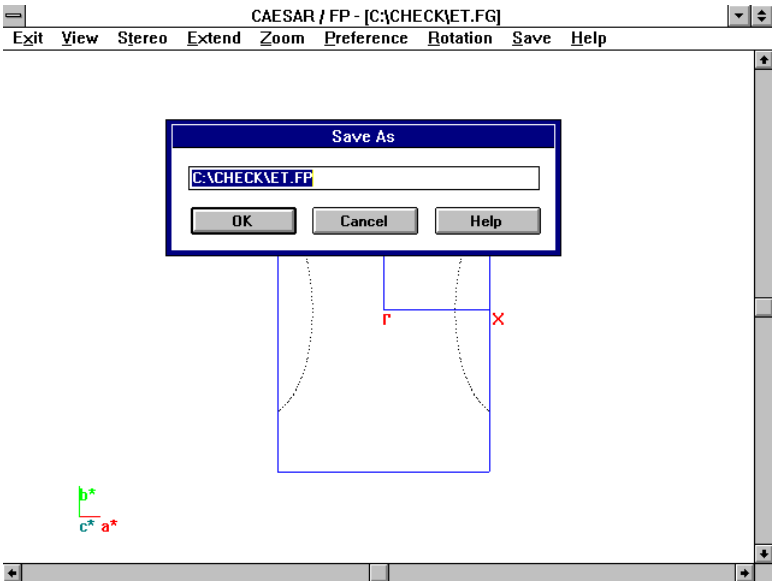

Figure 8.19. Save As dialog box for saving a picture.

8.3.2 Limitations of *FP*

The only limitation of *FP* is the maximum number of $\mathbf{k}_f$-points depicted within the FPZ. This is set at 20,000. When the *Extend* option is used to show more cells in the reciprocal space, only the $\mathbf{k}_f$-

points of the FPZ are counted.

8.4 Examples

8.4.1 $(BEDT\text{-}TTF)_2KHg(SCN)_4$ and $(BEDT\text{-}TSF)_2KHg(SCN)_4$ [1]

Organic conducting salts $(BEDT\text{-}TTF)_2MHg(SCN)_4$, where M = K, Rb, Tl, and NH_4, have been the subject of numerous magnetoresistance studies.[2,3] Shubnikov-de Haas and angle dependent magnetoresistance oscillations observed from magnetoresistance experiments provide invaluable experimental information about the shape of a Fermi surface. The angle dependent magnetoresistance oscillation (AMRO)data of $(BEDT\text{-}TTF)_2MHg(SCN)_4$ have been explained in terms of a circular 2D Fermi surface pocket and a pair of 1D Fermi surface lines. However, recent studies suggested that the observed AMRO data are better explained if the 2D Fermi surface pocket is significantly elliptical,[4,5] and the long axis of the ellipse is not parallel to the a*-direction.[5] To confirm these observations, electronic band structure calculations were performed for the $(BEDT\text{-}TTF)_2KHg(SCN)_4$ and $(BEDT\text{-}TSF)_2KHg(SCN)_4$ salts, and their Fermi surfaces were analyzed.[1] Here BEDT-TSF represents the organic donor molecule, bis(ethylenedithio)tetraselenafulvalene (*Figure 8.20*).

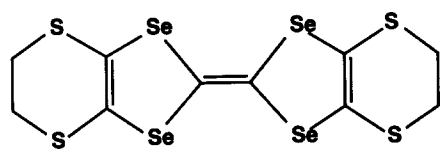

Figure 8.20. Structure of BEDT-TSF.

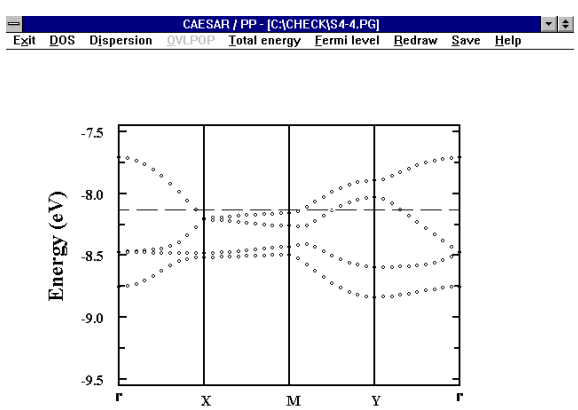

Figure 8.21. (a) Dispersion relations of the four highest occupied bands of $(BEDT\text{-}TTF)_2KHg(SCN)_4$, where the Fermi level is shown by the dashed line

In the CAESAR\Examples\Chapter8\BETS directory, the structural information for the $(BEDT\text{-}TTF)_2KHg(SCN)_4$ and $(BEDT\text{-}TSF)_2KHg(SCN)_4$ salts is given in *T.CI* and *S.CI*, respectively. The *BC*, *PC* and *FC* input files for $(BEDT\text{-}TTF)_2KHg(SCN)_4$ are given in *T.BI*, *T.PI* and *T.FI*,

respectively, and those for (BEDT-TSF)$_2$KHg(SCN)$_4$ in *S.BI*, *S.PI* and *S.FI*, respectively. The dispersion relations of the bands calculated for an isolated cation layer of (BEDT-TTF)$_2$KHg(SCN)$_4$ are shown in *Figure 8.21a*, and those of (BEDT-TSF)$_2$KHg(SCN)$_4$ in *Figure 8.22a*. For simplicity, only the four bands largely described by the HOMO's of the donor molecule are shown in each case. The dashed lines in *Figures 8.21a* and *8.22a* are the Fermi levels corresponding to the electron counting [(BEDT-TTF)$_2$]$^+$ and [(BEDT-TTF)$_2$]$^+$ per unit cell, respectively.

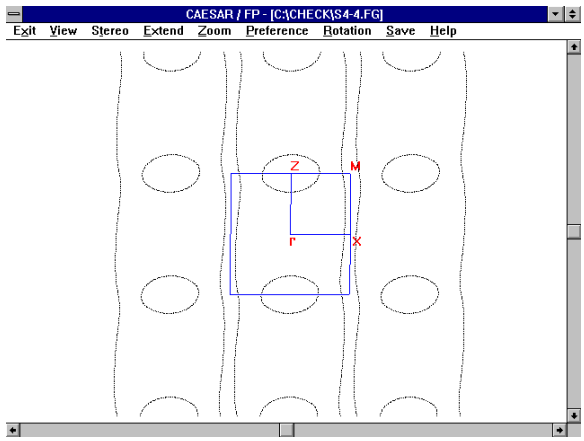

Figure 8.21. (b) Fermi surfaces associated with the partially filled bands of (BEDT-TTF)$_2$KHg(SCN)$_4$.

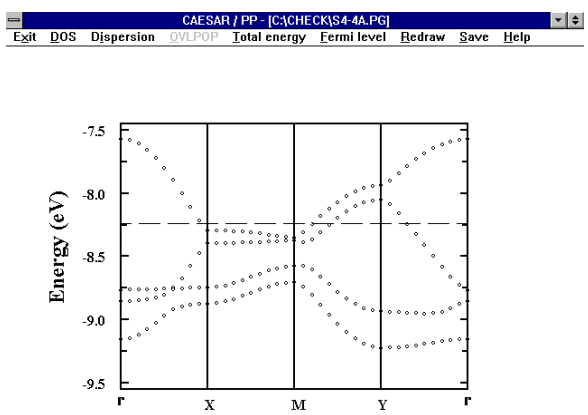

Figure 8.22. (a) Dispersion relations of the four highest occupied bands of (BEDT-TSF)$_2$KHg(SCN)$_4$, where the Fermi level is shown by the dashed line.

The Fermi surfaces associated with the partially filed bands of *Figures 8.21a* and *8.22a* are shown in *Figures 8.21b* and *8.22b*, respectively. Each Fermi surface consists of an ellipse centered at Z and a pair of lines straddling along the X-M line. *Figures 8.21b* and *8.22b* show that the (BEDT-TTF)$_2$KHg(SCN)$_4$ salt has more warped 1D Fermi surface pieces than does the (BEDT-TSF)$_2$KHg(SCN)$_4$ analog, so the nesting of the 1D Fermi surface is less favorable in the BEDT-TSF salt. The same trend is also found for the salts with M = NH$_4$.[1] This can bring about important

differences in the magnetoresistance properties of the BEDT-TTF and BEDT-TSF salts because the nesting of the 1D Fermi surfaces pieces is essential for the Fermi surface reconstruction in the (BEDT-TTF)$_2$KHg(SCN)$_4$.[3,4] Therefore, Fermi surface reconstruction is less likely to occur in the (BEDT-TSF)$_2$KHg(SCN)$_4$ salt.

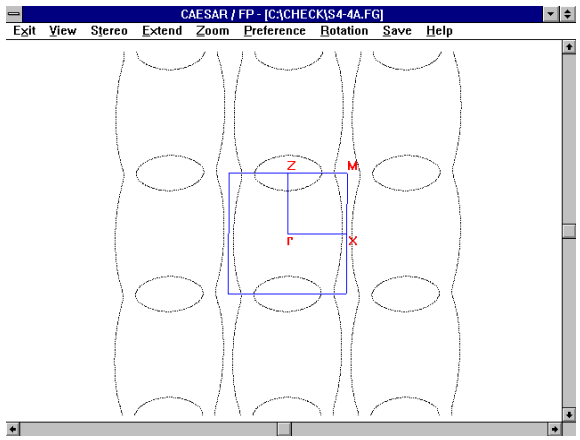

Figure 8.22. (b) Fermi surfaces associated with the partially filled bands of (BEDT-TSF)$_2$KHg(SCN)$_4$.

All 2D hole pockets of the BEDT-TTF and BEDT-TSF salts are elliptical, in agreement with experiment.[4,5] Each 2D hole pocket can be characterized by the size S (in percentage of the FPZ area), by the ellipticity r_L/r_S (here r_L and r_S are the long and short axes of an ellipse, respectively), and by the rotation θ around the axis which is perpendicular to the a*c*-plane and passes through the Z-point. (Here the sense of rotation is counterclockwise with $\theta = 0°$ when the long axis of the ellipse is parallel to Y-M line). The calculated S for (BEDT-TTF)$_2$KHg(SCN)$_4$ and (BEDT-TSF)$_2$KHg(SCN)$_4$ are 11.63 % and 12.79 %, respectively, which are comparable to the experimental observations of 15.4% and 15.8 %.[2,5] The BEDT-TSF salt has considerably more elliptical pocket ($r_L/r_S = 1.9$) than do the BEDT-TTF salt ($r_L/r_S = 1.5$). The rotation θ of the ellipse is substantial for the BEDT-TTF salt ($\theta = 9°$), in agreement with experiment.[4] This rotation is negligible for the BEDT-TSF salts ($\theta = 2°$).

8.4.2 κ-(BEDT-TTF)$_2$Cu(NCS)$_2$ [6,7]

As already discussed, each layer of BEDT-TTF molecules in κ-(BEDT-TTF)$_2$Cu(NCS)$_2$ is parallel to the crystallographic bc-plane.[8] In the CAESAR\Examples\Chapter8\ET directory, the *BC*, *PC* and *FI* input files for an isolated donor-molecule layer are *D.BI*, *D.PI* and *D.FI*, respectively.

Figure 8.23 shows the Fermi surfaces in an extended zone. To obtain this picture, it was necessary (1) to change the labels of symmetry points by using the *Unit cell box* command of the *Preference* menu and then selecting the item *yz(2D)* to switch the symmetry labels from 'X' and 'Y' to 'Y' and 'Z', respectively, (2) to use the *Zoom* command and select the option *Zoom Out 25%* to reduce its size, and (3) then to click the *5x5* command of the *Extend* menu.

The Fermi surfaces of κ-(BEDT-TTF)$_2$Cu(NCS)$_2$ in *Figure 8.23* are essentially described as overlapping distorted circles and these circles split into wavy lines and small elongated ellipses due to a noncrossing at the intended crossing points, which reflect that this salt has two non-equivalent BEDT-

FFT molecules. More explicitly, the Fermi surface of κ-(BEDT-TTF)$_2$Cu(NCS)$_2$ contains the hole surface (*Figure 8.24a*) and the electron surface (*Figure 8.24b*), which are respectively associated with the lower and upper subbands of the highest occupied band.

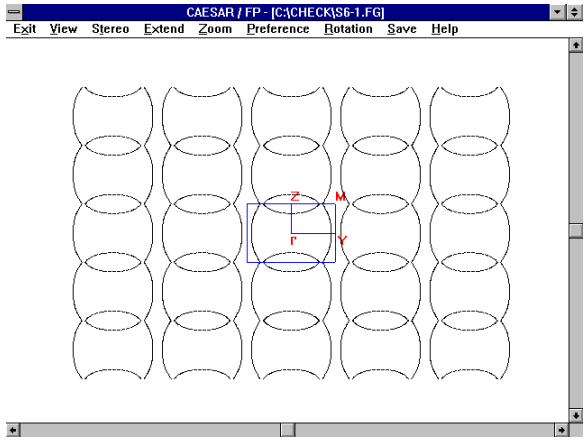

Figure 8.23. Fermi surfaces of k-(BEDT-TTF)$_2$Cu(NCS)$_2$ in an extended zone.

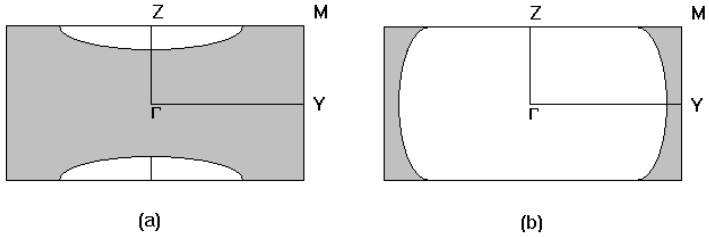

Figure 8.24. Schematic plots of the (a) hole and (b) electron Fermi surfaces of k-(BEDT-TTF)$_2$Cu(NCS)$_2$, where the occupied wave vectors are indicated by shading.

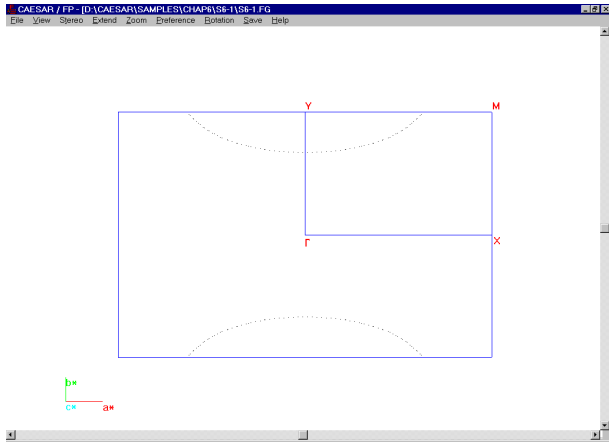

Figure 8.25. (a) Hole Fermi surfaces of k-(BEDT-TTF)$_2$Cu(NCS)$_2$.

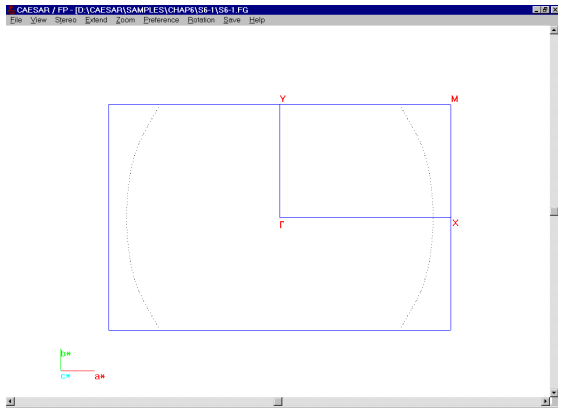

Figure 8.25. (b) electron Fermi surfaces of k-(BEDT-TTF)$_2$Cu (NCS)$_2$.

By using the *Area/Mass* command of the *Preference* menu, one can obtain the areas of the filled and empty regions of the hole and the electron Fermi surfaces as shown in *Figures 8.25a* and *8.25b*. This command opens the *Area/Mass information* dialog box (*Figure 8.26a*), which describes the hole Fermi surface generated by the band #191 (*Figure 8.25a*), and that of *Figure 8.26b* describes the electron Fermi surface generated by the band #192 (*Figure 8.25b*). These are consistent with the results of thermoelectric power measurements that the nature of the carrier is hole-like along the Γ→Z direction (i.e., the crystallographic c-direction), but electron-like along the Γ→Y direction (i.e., the crystallographic b-direction).[9]

The area of the hole surface (unshaded part in *Figure 8.24a*) is 13.56% of the FPZ (*Figure 8.26a)*, and that of the electron surface (shaded part in *Figure 8.24b*) is 19.68% of the FPZ (*Figure 8.26b)*. In principle, the electron and hole areas should be identical because electrons and holes are generated when the top of a completely filled band overlaps the bottom of a completely empty band. The electron area is slightly larger than the hole area, i.e., there are more electrons than holes. This is so because the Fermi level used calculations lies slightly higher than the true Fermi level. In the *BC* and *PC* programs, the Fermi levels are calculated by counting the number of electrons in the band energy levels generated for a set of k-points. Therefore, the calculated Fermi levels may deviate slightly from the true Fermi levels, in particular for the purpose of calculating the number of electrons and holes in semimetallic systems. For such cases, one simply needs to shift the Fermi level slightly until one obtains the same number of electrons and holes.

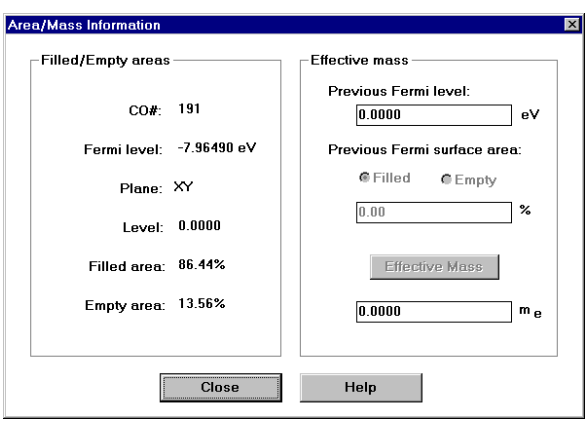

Figure 8.26. (a) Information about the hole Fermi surfaces of k-(BEDT-TTF)$_2$Cu(NCS)$_2$.

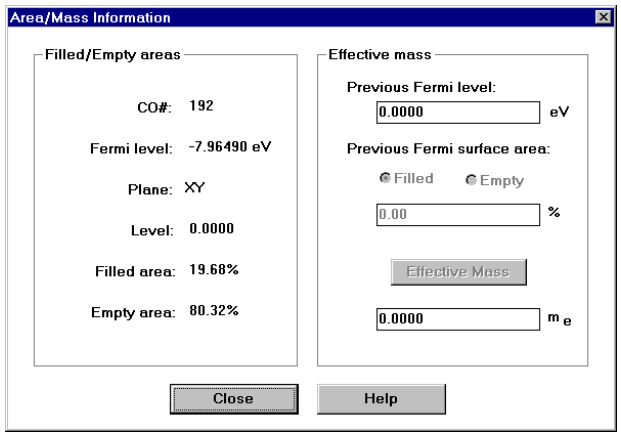

Figure 8.26. (b) Information about the electron Fermi surfaces of k-(BEDT-TTF)$_2$Cu(NCS)$_2$.

As explained in *Section 8.3.1*, the effective mass of the hole surface can be estimated by calculating how much the filled (or empty) area changes as the Fermi level is lowered or raised by a small amount (e.g., 0.1 eV). Such a calculation shows that the hole surface has the effective mass of 0.67 m_e.

8.4.3 K_xWO_3 [10]

As discussed in *Section 7.5.4*, K_xWO_3 has three partially filled d-block bands (*a*, *b* and *c* in *Figure 7.36*). *Band a* leads to 1D Fermi surface, and hence is responsible for the CDW phenomenon of K_xWO_3. The *BC*, *PC* and *FC* input files *FS.BI*, *FS.PI*, *FS1.FI*, *FS2.FI and FS3.FI* in the CAESAR\Examples\Chapter8\KxWo3 directory are designed to determine the Fermi surfaces of the $[WO_3]^{x-}$ lattice. *Figures 8.27a-c* show the 1D Fermi surfaces for x = 0.18, 0.25 and 1/3, respectively. For x = 0.25 and 1/3, this Fermi surface consists of two warped sheets perpendicular to the c*-direction. Thus, *band a* provides a 1D metallic character along the c-direction, as expected from the dispersion relations in *Figure 7.36*. As x varies from 1/3 to 0.25 to 0.18, the extent of warping increases in the 1D Fermi surface sheets. At x = 0.18, the two sheets are merged together around the K point through a funnel-like structure. Thus, the 1D character of *band a* increases as x increases from 0.18 to 1/3. The quasi 1D Fermi surface provides an approximate nesting and can give rise to a CDW instability. As x increases from 0.18 to 1/3, the average spacing between the two Fermi surface sheets in *Figures 8.27a-c* increases gradually. The nesting vector **q** determined from the well-nested regions (around X and M) is ~0.5**c*** for x = 0.25, which gives rise to a nearly "half filled" character for *band a*. For x = 0.18 and x = 1/3, the nesting vectors can be approximated by **q** = ~(0.5-ε)**c*** and ~(0.5+ε)**c***, respectively, where ε is a small positive number.

The calculated Fermi surface nesting vector **q** = ~0.5**c*** is consistent with the observed superlattice reflection peaks of A_xWO_3 (A = K, Rb). However, Cs_xWO_3 does not undergo a CDW transition although it has a 1D Fermi surface as do K_xWO_3 and Rb_xWO_3. To understand this difference, one should note that a CDW formation involves a periodic lattice distortion, which strains the lattice and hence destabilizes it.[11,12] Thus, a lattice cannot undergo a CDW transition unless the electronic energy gain dominates over the destabilization caused by the lattice strain. A CDW formation would be favorable for a system with soft lattice. As the lattice becomes stiffer, the CDW formation would become less favorable and hence occur at a lower temperature. The crystal structure of A_xWO_3 (A = K, Rb, Cs) suggests that the stiffness of the 3D WO_3 lattice should increase as more alkali atom sites are occupied, and that for a given x value the stiffness of the lattice should increase in

the order K_xWO_3 < Rb_xWO_3 < Cs_xWO_3, because the cation size increases in the order K^+ < Rb^+ < Cs^+. The lack of a CDW transition in Cs_xWO_3 implies that its lattice is too stiff to accommodate a

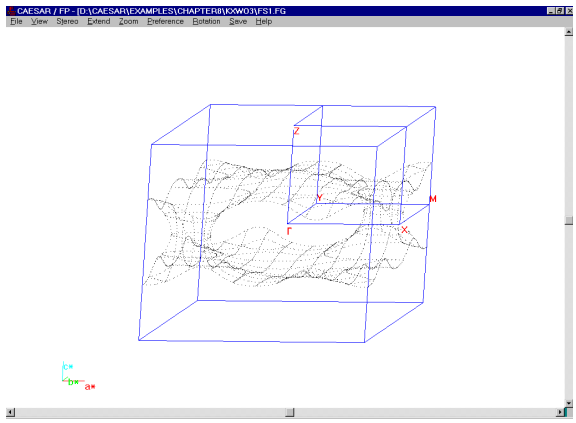

(a)

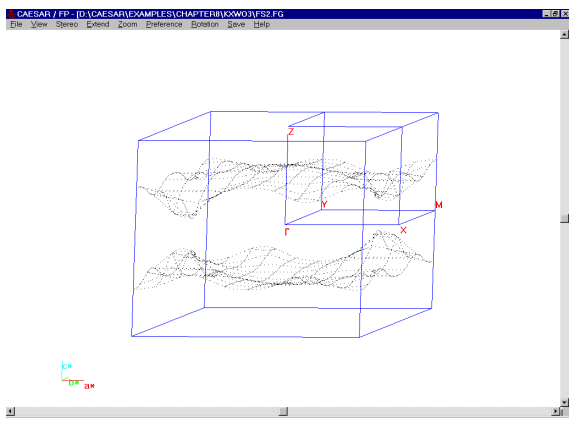

(b)

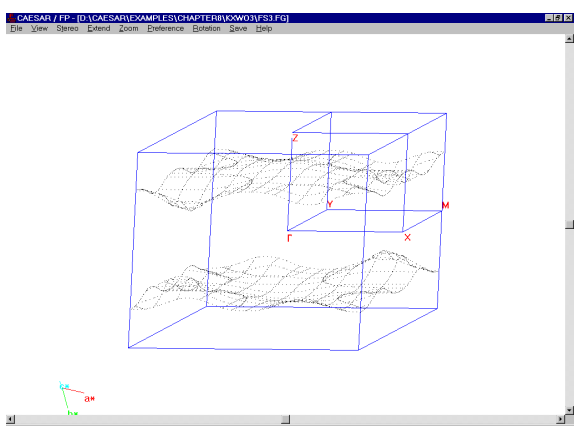

(c)

Figure 8.27. Fermi surfaces of the $[WO_3]^{x-}$ lattice for x = (a) 0.18, (b) 0.25 and (c) 1/3.

CDW formation. The occurrence of a CDW in K_xWO_3 and Rb_xWO_3 is consistent with the assertion that their lattices are less stiff than that of Cs_xWO_3. Since the WO_3 lattice should be less stiff for K_xWO_3 than for Rb_xWO_3, a CDW formation would be more favorable for K_xWO_3. This explains why the CDW onset temperature T_B of K_xWO_3 is higher than that of Rb_xWO_3 for most x values. In A_xWO_3 the stiffness of the WO_3 lattice should increase with increasing x from 0.18 to 1/3. This effect predicts the T_B to decrease gradually as x increases. However, the electronic instability associated with the 1D band predicts the T_B to increase gradually as x increases from 0.18 to 1/3. That is, the electronic instability and the lattice stiffness have opposing influences on the T_B-vs.-x relation. The occurrence of a maximum in the T_B-vs.-x plots can be considered a consequence of the two opposing effects. Then the electronic instability dominates when $x < 0.25$, while the lattice stiffness does when $x > 0.25$.

References

1. Seo; D.-K. Whangbo; M.-H. Fravel; B. Montgomwry; L. K. *Solid State Commun.* **1996**, *100*, 191.
2. Sasaki; T. Toyota; N. Tokomoto; M. Kinishita; N. Anzai; H. *Solid State Commun.* **1990**, *75*, 901.
3. Kartsovnik; M. V. Kovalev; A. E. Laukhin; V. N. Kushch; N. D., *J. Phys. I (France)* **1993**, *3*, 1187.
4. Brooks; J. S. Athas; G. J. Klepper; S. J. Chen; X. Campos; C. E. Valfells; S. Tanaka; Y. Kinoshita; T. Kinoshita; N. Tokomoto; M. Anzai; H. *Physica* **1994**, *B201*, 449.
5. House, A. A.; Blundell, S. J.; Honold, M. M.; Singleton, J.; Perenboom, J. A. A. J.; Hayes, W.; Kurmoo, M.; Day, P., *J. Phys. Condensed Matter*, **1996**, *8*, 8829.
6. William, J. M.; Ferraro, J. R.; Thorn, R. J.; Carlson, K. D.; Geiser. U.; Wang, H. H.; Kini, A. M.; Whangbo, M.-H. *Organic Superconductors (Including Fullenrenes)*, Prentice Hall, Englewood Cliffs, New Jersey, 1992, pp.265-267.
7. Kresin, V. Z.; Little, W. A., Eds. *Organic Superconductivity*, Plenum, New York, 1990, pp.254-259.
8. Jung, D.; Evain, M.; Novoa, J. J.; Whangbo. M.-H.; Beno, M. A.; Kini, A. M.; Schultz, A. J.; Williams, J. M.; Nigrey, P. J. *Inorg. Chem.* **1989**, *28*, 4516.
9. Urayama, H.; Yamochi, H.; Saito, G.; Sugano, T.; Kinoshita, M.; Inabe, T.; Mori, T.; Maruyama, Y.; Inokuchi, H. *Chem. Lett*. **1988**, 1057.
10. Lee, K.-S.; Seo, D.-K.; Whangbo, M.-H. *J. Am. Chem. Soc*. 1997, 119, 4043.
11. Whangbo, M.-H; Canadell, E. *J. Am. Chem. Soc*. **1992**, *114*, 9587.
12. Whangbo, M.-H.; Seo, D.-K.; Canadell, E., in *Physics and Chemistry of Low-Dimensional Inorganic Conductors*; Schlenker, C., Dumas, J., Greenblatt, M., van Smaalen, S., Eds.; Plenum; New York, 1996; p. 285.